Chemosphere 176 (2017) 255–265

Contents lists available at ScienceDirect

Chemosphere

journal homepage: www.elsevier.com/locate/chemosphere

Effects of polyphosphates and orthophosphate on the dissolution and transformation of ZnO nanoparticles

Biao Wan [a], Yupeng Yan [a], Yuanzhi Tang [b], Yuge Bai [a], Fan Liu [a], Wenfeng Tan [a], Qiaoyun Huang [a], Xionghan Feng [a, *]

[a] Key Laboratory of Arable Land Conservation (Middle and Lower Reaches of Yangtze River), Ministry of Agriculture, College of Resources and Environment, Huazhong Agricultural University, Wuhan, 430070, China
[b] School of Earth and Atmospheric Sciences, Georgia Institute of Technology, 311 Ferst Dr, Atlanta, GA 30324-0340, USA

HIGHLIGHTS

- Polyphosphates affect the speciation and transformation of ZnO NPs through multiple processes.
- The interactions of ZnO NPs with P_1, P_2, and P_3 formed Zn-P precipitates.
- P_6 promoted the dissolution of ZnO NPs via the formation of soluble Zn-P_6 complexes.
- The transformation of ZnO NPs was affected by reaction time, pH, and P/Zn molar ratio.
- New insights for understanding the uptake of P compounds by ZnO NPs via enhanced particle dissolution and transformation.

GRAPHICAL ABSTRACT

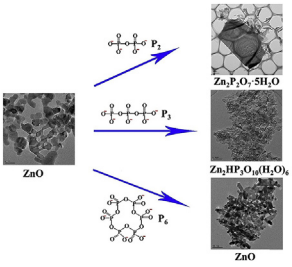

ARTICLE INFO

Article history:
Received 15 July 2016
Received in revised form
11 February 2017
Accepted 25 February 2017
Available online 27 February 2017

Handling Editor: Chang-Ping Yu

Keywords:
Polyphosphates
Orthophosphate
ZnO nanoparticles
Dissolution
Transformation
Natural environment

ABSTRACT

The fate and toxicity of zinc oxide nanoparticles (ZnO NPs) in nature are affected by solution chemistry such as pH, anions, and natural organic matter (NOM). Inorganic polyphosphates are environmentally ubiquitous phosphorus (P) species that may change the speciation and environmental fate of ZnO NPs. In this study, the interactions of polyphosphates with ZnO NPs and the impacts on ZnO NP dissolution and transformation were investigated and compared with orthophosphate (P_1). The results revealed that pyrophosphate (P_2), tripolyphosphate (P_3), and hexametaphosphate (P_6) enhanced whereas P_1 inhibited the dissolution of ZnO NPs. In addition, P_1, P_2, and P_3 promoted the transformation of ZnO NPs into zinc phosphate (Zn-P) precipitates via interactions with dissolved Zn^{2+}. However, P_6-promoted ZnO NP dissolution was through the formation of soluble Zn-P complexes due to the strong capability of P_6 to chelate with Zn^{2+}. The transformation of ZnO NPs in the presence of P_3 was affected by reaction time, pH, and P/Zn molar ratio. P_3 first formed inner-sphere surface complexes on ZnO NPs, which gradually transformed into crystalline $Zn_2HP_3O_{10}(H_2O)_6$ precipitates. This study provided a new perspective for understanding the reactivity of various forms of inorganic phosphate species with ZnO NPs in the natural environment.

* Corresponding author.
E-mail address: fxh73@mail.hzau.edu.cn (X. Feng).

http://dx.doi.org/10.1016/j.chemosphere.2017.02.134
0045-6535/

1. Introduction

The large production and widespread applications of manufactured engineering nanoparticles (ENPs) would inevitably result in their release into the environment, yet uncertainties still exist regarding their environmental fate and impacts (Klaine et al., 2008). ZnO NPs are the second most produced nanomaterials with wide commercial and environmental applications, such as catalysis, sunscreen, industrial coatings, and antibacterial agents (Keller and Lazareva, 2014; Kołodziejczak-Radzimska and Jesionowski, 2014). Consequently, ZnO NPs are likely to be released into municipal wastewater, natural waterbodies, and soils (Gottschalk et al., 2009; Keller and Lazareva, 2014). The concentrations of ZnO NPs in surface waters, sewage influent, sewage effluent, sewage sludge, sediments, and soils were approximately estimated to be 0.001–0.61 μg L^{-1}, 24–300 μg L^{-1}, 0.05–45 μg L^{-1}, 13.6–200 mg kg^{-1}, 0.02–1.0 mg kg^{-1}, and 0.01–10 μg kg^{-1}, respectively (Barton et al., 2015; Gottschalk et al., 2009, 2013; Sun et al., 2014; Zhang et al., 2017). ZnO NPs have relatively high toxicity (at the low mg L^{-1} levels) to many organisms, such as bacteria, algae, plants, as well as aquatic and terrestrial invertebrates and vertebrates (Pandurangan and Kim, 2015; Wang et al., 2013). The primary mechanisms of ZnO NP induced toxicity are the dissolution and release of Zn^{2+} and NP-induced generation of reactive oxygen species (ROS) (Ma et al., 2013a). As an inorganic material, many previous studies of ZnO NPs were primarily focused on their physical (*e.g.*, aggregation and sedimentation) and chemical (*e.g.*, dissolution and sulfidation) transformations (Bian et al., 2011; Keller et al., 2010; Ma et al., 2013b). Ionic strength, pH, particle size, existence of anions (*e.g.*, carbonate and phosphate), and adsorption onto NOM can all impact the physico-chemical properties (*e.g.*, colloidal stability, aggregation, and dissolution) of ZnO NPs and their subsequent environmental fate and ecotoxicity (Bian et al., 2011; Keller et al., 2010; Li et al., 2013; Reed et al., 2012). For example, the presence of phosphate and NOM can decrease the dissolution of ZnO NPs and thus lower their toxicity to *Escherichia coli* due to the decrease of free Zn^{2+} concentration (Li et al., 2013). Therefore, it is important to understand the dissolution and transformation of ZnO NPs in natural medium, which will provide fundamental basis for better predicting their behavior and fate in natural and engineered environments (Lowry et al., 2012; Sivry et al., 2014).

Phosphorus (P) is a critical element for all living protoplasmic organisms and can enrich in certain natural environments and industrial effluents (Arai and Sparks, 2007). The main forms of P-containing compounds are orthophosphate (P_1), organic P, polyphosphates, and metaphosphates (Arai and Sparks, 2007). One condensed form of inorganic P is polyphosphates, which are molecules formed by two or more phosphate groups via O–P–O linkages and can be linear or cyclic (also called metaphosphates) in structure. Polyphosphates exist in the natural and wastewater treatment systems (Arai and Sparks, 2007; Huang and Tang, 2015; Worsfold et al., 2008). Natural sediment of lakes, estuaries and oceans also contain a wide range of P species such as P_1, polyphosphates, and phosphate monoesters and diesters (Diaz et al., 2008; Worsfold et al., 2008). In the granule sludge, polyphosphates are a group of important P species besides the dominating orthophosphate (Huang et al., 2015). Finstein and Hunter (1967) reported that polyphosphates accounted for approximately 15–75% of the total phosphorus in raw sewage sludge and 5–40% of that in secondary effluents (Finstein and Hunter, 1967).

Polyphosphates are conserved by almost all organisms in nature (*e.g.*, bacteria, fungi, plants, and animals) and are thought to play unique roles in the origin and survival of species (Rao et al., 2009). A large number of polyphosphates are also used in detergents, mainly in the form of sodium triphosphate (P_3) (30–35%) and are eventually discharged into wastewater treatment plants (Guan et al., 2005; Lampronti et al., 2012). P_3 can hydrolyze to form pyrophosphate (P_2) and P_1 in the washing machine water system (Lampronti et al., 2012). Pyrophosphate can also form non-enzymatically via coupled exergonic hydrolysis of P_3 and endergonic condensation of P_1 at room temperature under neutral/alkaline pHs (Uchimiya and Hiradate, 2014). Therefore these different P compounds are expected to co-exist with ZnO NPs in systems such as municipal wastewater (and treatment systems) and natural waterbodies (Brunetti et al., 2015; Huang et al., 2015) and the interaction between them might be inevitable. Previous investigation pointed out that high concentrations (50 mg L^{-1}) of ZnO NPs inhibited P removal in wastewater treatment plants (WWTPs) due to the release of Zn^{2+} and increase of ROS production (Zheng et al., 2011). However, this study did not consider the precipitation between P and dissolved Zn^{2+} and its impact on P removal. Studies have confirmed that P_1 can induce the transformation of ZnO NPs to tetrahydrate $Zn_3(PO_4)_2$ under neutral pH conditions (Lv et al., 2012), and such transformation was pH dependent in that crystalline hopeite ($Zn_3(PO_4)_2 \cdot 4H_2O$) preferred to form at pH 6.0 rather than pH 8.0 (Rathnayake et al., 2014). It was recently found that ZnO NPs was converted to Zn-phosphate compounds in sewerage networks (Brunetti et al., 2015), but the possible effect of O–P–O linkages on the microstructural transformation of ZnO NPs as well as the main components in Zn-phosphate phase are still unclear. Revealing the interaction of ZnO with different forms of P is thus important for understanding the transformation mechanisms and kinetics of ZnO NPs under P-enriched conditions.

In this study, the dissolution and transformation of ZnO NPs in the presence of orthophosphate and several forms of polyphosphates (*i.e.*, pyrophosphate, tripolyphosphate, and hexametaphosphate) were investigated. To our knowledge, this is the first study investigating the microstructure and transformation processes of ZnO NPs with these inorganic P species with different chain lengths. The speciation and phase transformation of ZnO NPs were characterized by *in situ* attenuated total reflectance Fourier transform infrared (ATR-FTIR) spectroscopy, powder X-ray diffraction (XRD), and high-resolution transmission electron microscopy (HRTEM). Results of this study provide a better understanding of the behavior and fate of ZnO NPs in both natural ecosystems and industrial settings.

2. Experimental section

2.1. Materials

Sodium dihydrogen phosphate (NaH_2PO_4, P_1), disodium pyrophosphate dihydrate ($Na_2H_2P_2O_7 \cdot 2H_2O$, P_2), sodium tripolyphosphate ($Na_5P_3O_{10}$, P_3), and sodium hexametaphosphate ($(NaPO_3)_6$, P_6) were obtained from Sinopharm Chemical Reagent Co., Ltd. (Shanghai, China). The ZnO NPs (99.9% purity) were purchased from Nanjing Emperor Nano Material Co., Ltd. (Jiangsu, China) and contained no impurity phases without any surface coating materials as examined by powder XRD, FTIR and TEM analyses.

2.2. Reaction of ZnO NPs with polyphosphates and orthophosphate

Sorption kinetics experiments were conducted to understand the interaction between ZnO and four forms of P (P_1, P_2, P_3, and P_6) with total P/Zn molar ratio of 1:1 at pH 7.0. The interaction between ZnO NPs and P_3 was also investigated at different pH levels and different $P_{\_P3}$/Zn molar ratios (where $P_{\_P3}$ specifically refers to total P concentration added in the ZnO-P_3 system). pH values of the batch experiments were measured using a pH meter (FE20,

Mettler-Toledo, Shanghai, China). The solution pH was manually adjusted to desired pH values ± 0.2 using 0.1 M HCl and 0.1 M NaOH several times within the first 2 h. After that, the pH of each reaction suspension was adjusted at 3, 6, 9, 12, and 24 h. The reaction temperature was maintained at 25 ± 0.2 °C using a water circulator. ZnO NP powders (0.162 g) were mixed with 200 mL 0.01 mol L^{-1} NaCl solution containing P_1, P_2, P_3, and P_6 (10 mmol L^{-1} total P) at pH 7.0, or P_3 at different pHs (5.0, 7.0, and 9.0) and with various P_{-P3}/Zn molar ratios (0, 0.2, 0.5, and 1.0) at pH 7.0. At specific reaction time, a 5-mL suspension was filtered through a 0.22-μm Millipore membrane to analyze the solution concentration of P and Zn^{2+} in order to calculate P uptake and the concentration of Zn^{2+} dissolved from ZnO NPs. After 24 h of reaction, the remaining suspension was centrifuged (at 16,000 × *g* for 15 min), washed two times using P-free 0.01 mol L^{-1} NaCl solution at corresponding pH to remove the residual P. A portion of the recovered wet paste was directly examined by ATR-FTIR, and a portion was air dried for XRD and TEM analyses. Each experiment of P sorption kinetics was performed in duplicate. To measure total P concentration for experiments involving polyphosphates, polyphosphates were first hydrolyzed to orthophosphate using concentrated sulfuric and perchloric acid digestion (Martin et al., 1999), then measured using the phosphatemolybdate blue colorimetric method (Murphy and Riley, 1962). Concentration of dissolved Zn^{2+} in the supernatants was quantified using a 240FS atomic absorption spectrometer (AAS) (Varian, Palo Alto, USA). In addition, ZnO samples reacted with P_3 for various P loading (total P concentration = 2.0, 5.0, 10.0 mmol L^{-1}) at pH 7.0 and P_3 at various pHs (total P concentration = 10.0 mmol L^{-1}) were analyzed at different reaction time (1, 4, 10, and 24 h) and prepared for ATR-FTIR and XRD analyses as mentioned above.

2.3. Characterization of ZnO NPs and reaction products

Both unreacted and reacted ZnO NPs were characterized using a suite of complementary techniques. Sedimentation of unreacted ZnO NPs were examined by monitoring time-resolved optical absorbance at 378 nm using a UV–vis spectrophotometer (UV-6300PC, Shanghai, China) (Bian et al., 2011). The zeta (ζ) potentials of unreacted ZnO NPs were measured at different pHs (6.5–10.0) in 0.01 mol L^{-1} NaCl solution using a Malvern Zetasizer ZEN 3600 zeta potential analyzer (Malvern Instruments Ltd., Malvern, UK). The hydrodynamic diameter (z-average diameter) of pure ZnO NPs at pH 7.0 in 0.01 mol L^{-1} NaCl was measured by dynamic light scattering (DLS) (Malvern Zetasizer ZEN 3600). The specific surface area of ZnO NPs was measured by the Brunauer–Emmett–Teller (BET) method with an Autosorb-1 N_2 absorption analyzer (Quantachrome, Boynton Beach, FL, USA). The speciation and phase transformation of ZnO NPs were characterized by *in situ* ATR-FTIR spectroscopy (Bruker Vertex 70 FTIR spectrometer) and XRD (Bruker D8 Advance diffractometer). HRTEM analysis was carried on a JEM-2100F STEM/EDS (JEOL, Japan) at 200 kV, and the samples were prepared by spreading 10-μL aliquots of suspended ZnO NPs or reacted samples onto carbon-coated copper grids. Additional details on experimental conditions, analytical procedures, and characterization are provided in Supplementary Information (SI).

3. Results

3.1. Uptake of P and dissolution of ZnO NPs

Sorption of four forms of P (P_1, P_2, P_3 and P_6) onto ZnO NPs and their influence on the dissolution of ZnO NPs were studied over 24 h (Fig. 1). In general, at total P/Zn molar ratio of 1.0, the concentration changes of total P for various forms of P and dissolved Zn^{2+} change as reaction time increased. As shown in Fig. 1a, P uptake for P_1 increased gradually and reached equilibrium within 2–3 h. P uptake for P_2 increased dramatically and almost reached 100% (*i.e.*, 10 mmol L^{-1}) within 0.5–1 h. P uptake for P_3 increased slowly over 24 h, however, that for P_6 did not change within 24 h (Fig. 1a).

In the absence of P, moderate dissolution of ZnO NPs was observed at pH 7.0, and the concentration of dissolved Zn^{2+} was ~1.8 mmol L^{-1} (equal to 18% of total ZnO) at 10 h (Fig. S4). As shown in Fig. 1b, addition of P_1 into the suspension significantly decreased the concentration of dissolved Zn^{2+} to ~10 μmol L^{-1} (equal to 0.1% of total ZnO) at 24 h. In the presence of P_2, the concentration of dissolved Zn^{2+} was initially very high (~2.1 mmol L^{-1}, equal to 21% of total ZnO), but decreased dramatically over time and reached a steady state of ~0.1 mmol L^{-1} (equal to 1% of total ZnO). In the presence of P_3, the concentration of dissolved Zn^{2+} first increased and reached a maximum concentration of 2.2 mmol L^{-1} (equal to 22% of total ZnO) at 4 h, then decreased gradually and eventually reached a steady state of 1 mmol L^{-1} (10% of total ZnO) at 24 h. The concentration of dissolved Zn^{2+} in the presence of P_6 was very high and always around 5 mmol L^{-1} (equal to 50% of total ZnO) over the 24 h reaction time. The equilibrium concentration of dissolved Zn^{2+} for P_1, P_2 and P_6 systems are ~0.1, ~0.1 and ~5 mmol L^{-1}, respectively. The equilibrium concentration of corresponding total P in these systems are ~3.3, ~0, and ~9.6 mmol L^{-1}, respectively. Based on these observations, we hypothesize that (1) P_1 likely converted directly to Zn-P_1 precipitates as P_1 does not have the ability to chelate metal ions (Lv et al., 2012; Rathnayake et al., 2014); (2) P_6 likely formed soluble Zn-P_6 complexes which significantly increased the concentration of dissolved Zn^{2+} (Omelon and Grynpas, 2011); and (3) P_2 and P_3 might have initially complex with Zn^{2+} and induce the dissolution of ZnO NPs that resulted in the increasing concentration of dissolved Zn^{2+}; and then, the formed Zn-P_2/P_3 complexes gradually transformed into insoluble Zn-P_2/P_3 precipitates that decreased the concentration of dissolved Zn^{2+} (Feng et al., 2016; Michelmore et al., 2003).

In the presence of P_3, the influences of P_{-P3}/Zn molar ratios and solution pH on the transformation of ZnO NPs were further investigated (Fig. 1c, d and S6). At P_{-P3}/Zn molar ratio of 0.5, the Zn^{2+} concentration increased slowly within the first 8 h with a maximum dissolved Zn^{2+} concentration of 0.8 mmol L^{-1} (equal to 8% of total ZnO), then decreased gradually over time (Fig. 1d). At a P_{-P3}/Zn molar ratio of 0.2, the Zn^{2+} concentration was always around 0.4 mmol L^{-1} (equal to 4.0% of total ZnO) over the 24 h course (Fig. 1d). These results suggest that a small amount of surface P_3 coverage may inhibit the dissolution of ZnO NPs, possibly due to the formation of surface Zn-P_3 complexes/precipitates. The P uptake for P_3 (*e.g.*, loss of P_{-P3} in solution) followed a similar pattern for the three different P_{-P3}/Zn molar ratios, in that they all gradually increased over time (Fig. 1c). At pH 9.0 where ZnO NPs are typically insoluble (Feng et al., 2016), and the P_{-P3} concentration decreases to 9.3 mmol L^{-1} due to sorption of P_3 onto ZnO NPs (Fig. S6a) since the concentration of dissolved Zn^{2+} was close to zero. However, at pH 5.0 where ZnO NPs completely dissolves (Feng et al., 2016), the concentration of P_{-P3} was always lower than 1 mmol L^{-1}, and the Zn^{2+} concentration increased dramatically within the first 2 h, reaching 5.9 mmol L^{-1} (equal to 59% of total ZnO), then decreased gradually to 3 mmol L^{-1} (equal to 30% of total ZnO) (Fig. S6b). Due to the excellent chelate ability of P_3, it is hypothesized that a rapid complexing reaction might have taken place between Zn^{2+} and P_3, causing the increase of Zn^{2+} when P_3 was at high concentration, followed by the precipitation of the soluble Zn-P_3 complexes, resulting in the decrease of both dissolved Zn^{2+} and P_{-P3} in solution (Feng et al., 2016; Yan et al., 2014).

For the uptake of P onto ZnO NPs, not a single adsorption process

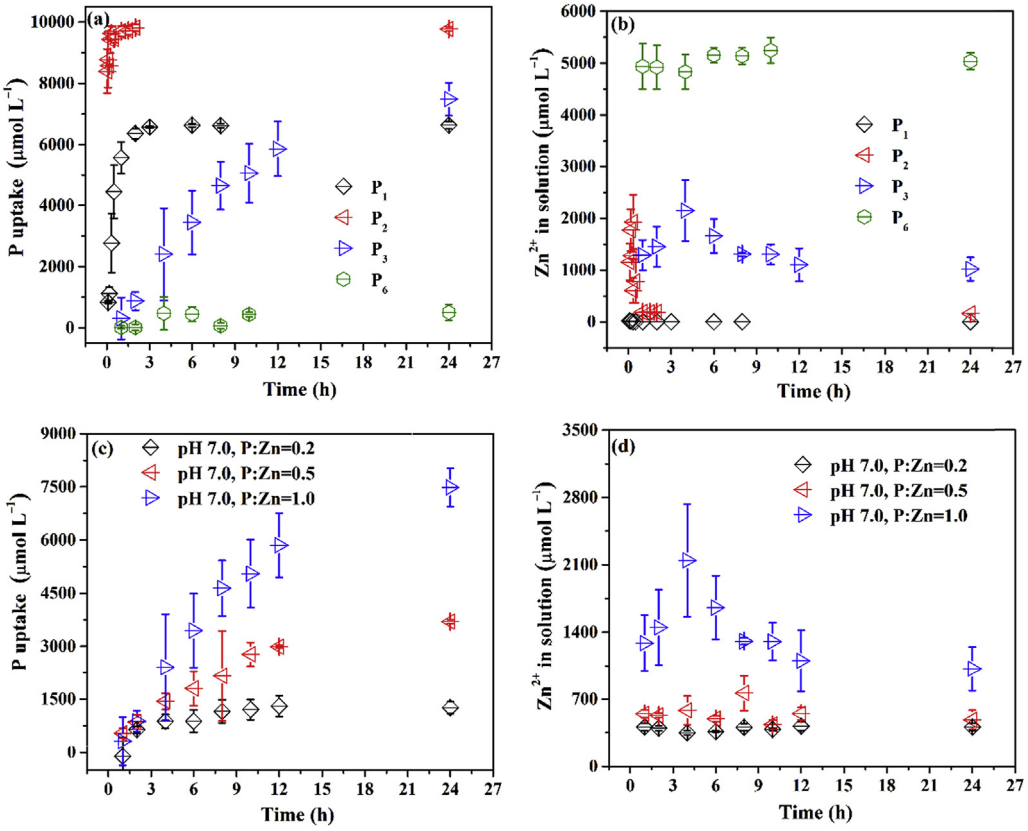

Fig. 1. Concentration of total P uptake (a) and dissolved Zn^{2+} (b) as a function of time upon ZnO NP reaction with four different P compounds (P_1, P_2, P_3, P_6) at a P/Zn molar ratio of 1.0. Concentration of P_{-P3} uptake (c) and dissolved Zn^{2+} (d) in solution as a function of time with P_{-P3}/Zn molar ratios of 0.2, 0.5 and 1.0. Each data point represents the mean of two replicate experiments with standard deviation shown by error bars.

but several reactions (*e.g.*, surface complexation, dissolution, and precipitation) occurred simultaneously between polyphosphates and ZnO NPs. This makes it difficult to model the reaction kinetics (Fig. 1 and S6) and the quantitative analyses of the P uptake and Zn dissolution data with physiochemical meanings are challenging. For the sake of simplicity, a pseudo-first-order kinetic model was used to describe P uptake data (Fig. 1a and c and S6a) to quantitatively compare P fixation/sequestration efficiencies of various P forms by ZnO NPs (Fig. S5). The kinetic model is $C_t = C_0 \times e^{-kt}{}_m$ or $\ln C_0 - \ln C_t = k_m t$, where C_0 (μmol L^{-1}) is the initial P concentration, C_t (μmol L^{-1}) is the total P concentration at a given time t (h), and k_m (h^{-1}) is the apparent rate constant. Before the complete transformation of ZnO NPs into Zn-P precipitates, a pseudo-first-order kinetic model could be used to describe sorption data of four P compounds onto ZnO NPs. The rate constants (k_m) are in the orders of 0.9585 h^{-1} (P_2) > 0.4821^{-1} (P_1) > 0.0596 h^{-1} (P_3) > 0.00018 h^{-1} (P_6) for the four P compounds at pH 7.0 (Fig. S5a); 0.0807 h^{-1} (0.2) > 0.073 h^{-1} (0.5) > 0.0596 h^{-1} (1.0) for P_3 with different P/Zn molar ratio (0.2, 0.5, and 1.0) at pH 7.0 (Fig. S5b); and 0.0977 h^{-1} (pH 5.0) > 0.0596 h^{-1} (pH 7.0) > 0.00015 h^{-1} (pH 9.0) for P_3 with P/Zn molar ratio of 1.0 at different pHs (5.0, 7.0, and 9.0) (Fig. S5c). Therefore, the uptake of P onto ZnO NPs was affected by reaction time, solution pHs, P/Zn molar ratio and the P forms.

3.2. XRD and ATR-FTIR analysis

XRD and ATR-FTIR were used to characterize the structure of ZnO NPs before and after reacting with P species. XRD patterns of ZnO NPs reacted with four forms of P were significantly different (Fig. 2). The XRD pattern of ZnO-P_6 sample showed sharp diffraction peaks at 2θ = 31.7, 34.4, and 36.1° (Fig. 2d), characteristic of crystalline hexagonal ZnO NPs (JCPDS No. 89–1397). For ZnO NPs-P_1 system (Fig. 3a), orthorhombic hopeite ($Zn_3(PO_4)_2 \cdot 4H_2O$) was indicated by peaks at 2θ values of 9.6, 16.6, 17.3, 18.2, 19.3, 20.08, 22.18, 26.17, 31.69, and 46° (JCPDS No. 37–0465). For ZnO NPs sample reacted with P_2 over 24 h (Fig. 2b), we observed evidences for a crystalline phase $Zn_2P_2O_7 \cdot 5H_2O$ (JCPDS No. 07–0087), which exhibited main diffraction peaks at 2θ = 6.9, 13.87, 15.93, 19.36, 19.98, 23.97, 25.35, 28.22 and 33.78°. When ZnO NPs aged in P_3 solution over 24 h, besides the presence of crystalline hexagonal ZnO NPs, XRD patterns also revealed sharp diffraction peaks at 2θ = 8.7, 9.29, 11.38, 11.69, 12.54, 20.98, 23.75, and 32.93° (Fig. 2c), which are characteristic of crystalline $Zn_2HP_3O_{10}(H_2O)_6$ (JCPDS No. 30–1478).

ATR-FTIR spectroscopy can provide molecular level insights into the adsorption/precipitation of P species at the surfaces of ZnO NPs. FTIR spectra of the P species in dissolved forms are illustrated in Fig. S7. Bands in the 1200–1300 cm^{-1} region can be assigned to the asymmetric stretching vibrations of the bridging PO_2^- (O=P–O^-) ($\nu_{as}(PO_2^-)$). Bands around 900 cm^{-1} for P_2, P_3, and P_6 belong to the asymmetric stretching vibration of P–O–P (ν_{as}(P–O–P)). Bands appearing in the 1080–1120 and 1000–1030 cm^{-1} regions can be assigned to the asymmetric and symmetric stretching vibrations of the PO_3^- ($\nu_{as}(PO_3^{2-})$ and $\nu_s(PO_3^{2-})$), respectively (Fig. 2e and S7) (Gong, 2001; Guan et al., 2005).

The FTIR spectra of the wet pastes after reactions are given in Fig. 3f, with peak assignments summarized in Table S2. FTIR spectra for non-reacted ZnO NPs showed a broad absorbance band at ~870 cm^{-1}. The spectra of the reacted products were quite different from those of their corresponding P species, indicating that the

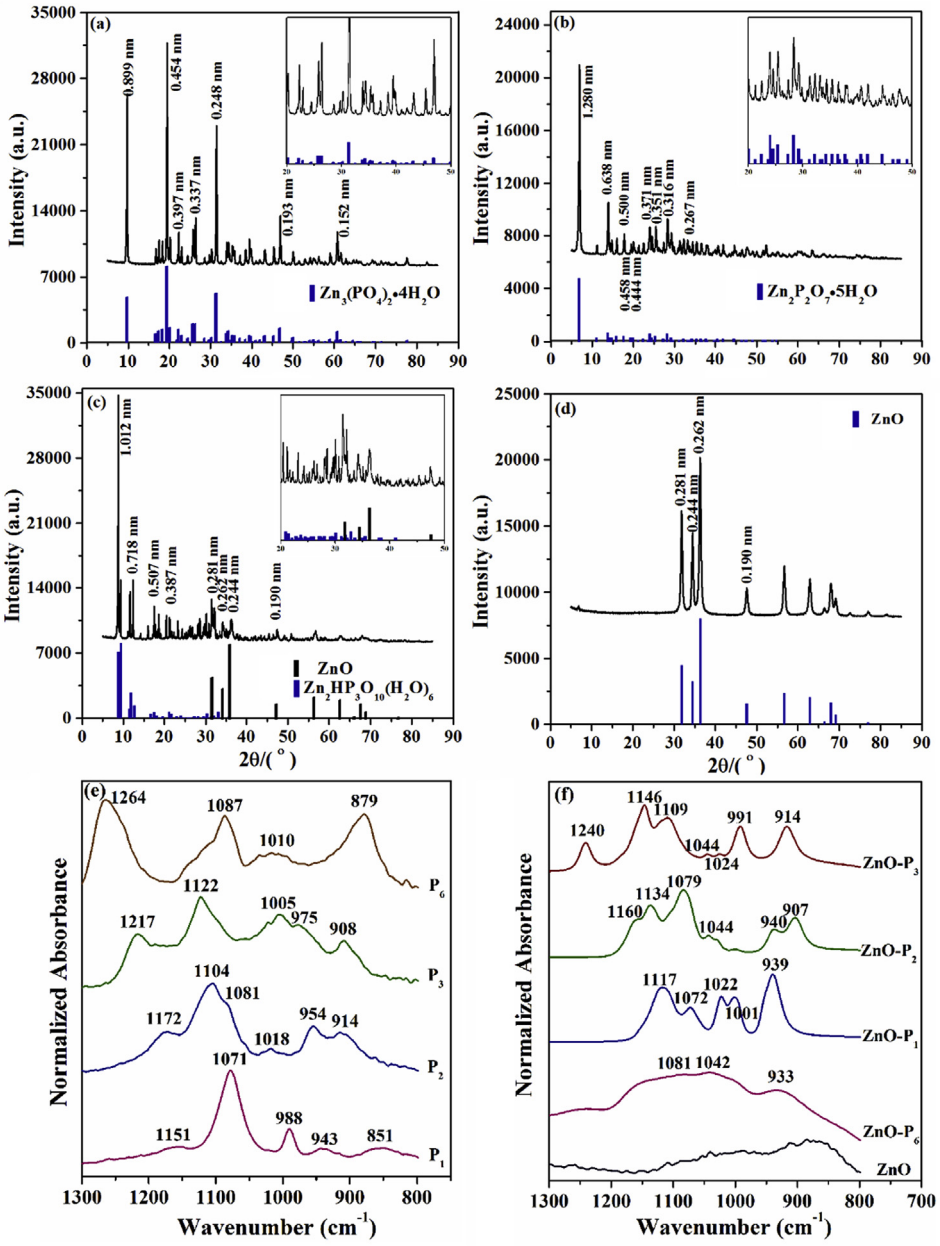

Fig. 2. XRD patterns of ZnO NPs reacted with P_1 (a), P_2 (b), P_3 (c) and P_6 (d) at pH 7.0. Zoom-in regions (20–50°) of P_1, P_2 and P_3 products reacted with ZnO NPs are shown as inserts. Normalized ATR-FTIR spectra of dissolved P_1, P_2, P_3, and P_6 before (e) and after reacted with ZnO NPs (f) at pH 7.0. Solutions of P_1, P_2, P_3, and P_6 (total P concentration) for FTIR measurements were prepared at 100 mmol L^{-1} in 0.01 mol^{-1} NaCl.

structural configuration of polyphosphates and orthophosphate were altered after reaction with ZnO NPs (Fig. 2e and f). For ZnO NPs aged in P_1 solution, there are five strong bands at 939, 1001, 1022, 1072 and 1117 cm^{-1} (Fig. 2f), similar to the spectra of $Zn_3(PO_4)_2$ (He et al., 2007). For ZnO NPs reacted with P_6, there are three bands at 933, 1042, and 1081 cm^{-1}, which may be assigned to ν_{as}(P–O–P), $\nu_s(PO_3)$, and $\nu_s(PO_2)$, respectively (Fig. 2f) (Michelmore et al., 2003). Six peaks at 1160, 1134, 1079, 1044, 940, and 907 cm^{-1} dominated the spectra of P_2-ZnO NPs system (Fig. 2f). Compared with the FTIR spectra of P_2 in solution, the peak corresponding to symmetric vibration of the terminal PO_3^{2-} shifted from 1018 to 1044 cm^{-1}, and the bands belonging to ν_{as} (P–O–P) split from 914 cm^{-1} to 907 and 940 cm^{-1} (Fig. 2e and f). Bands at 1160, 1134, and 1079 cm^{-1} can be assigned to $\nu_{as}(PO_2)$, ν_{as}(P–O in Zn–PO_3^-), and $\nu_{as}(PO_3)$, respectively (Assaaoudi et al., 2005; Guan et al., 2005; Michelmore et al., 2003). This result suggested that the IR vibration of reaction products involved the vibration of P–O and P–O–Zn, and that the reaction products is possibly $Zn_2P_2O_7 \cdot 5H_2O$ with additional evidence from XRD analysis (Fig. 2b). Finally, when ZnO NPs aged in P_3 solution over 24 h, seven peaks at 1240, 1146, 1109, 1044, 1024, 991, and 914 cm^{-1} dominated in the spectra of the reacted sample (Fig. 2f). The frequencies of $\nu_{as}(P_2O_7^{4-})$ and ν_{as}(P–O–P) remained unchanged in the spectra of P_3, but shifted moderately to a higher frequency upon P_3 interaction with ZnO NPs (Fig. 2e and f). Bands at 1146 and 1024 cm^{-1} can be assignment to ν_{as}(P–O in Zn–PO_3^-) and ν_{as}(P–OH in $HP_3O_{10}^{4-}$), respectively (Guan et al., 2005; Michelmore et al., 2003). Combined with XRD observation, these results suggested that the reaction products were $Zn_2HP_3O_{10}(H_2O)_6$ (Fig. 2c).

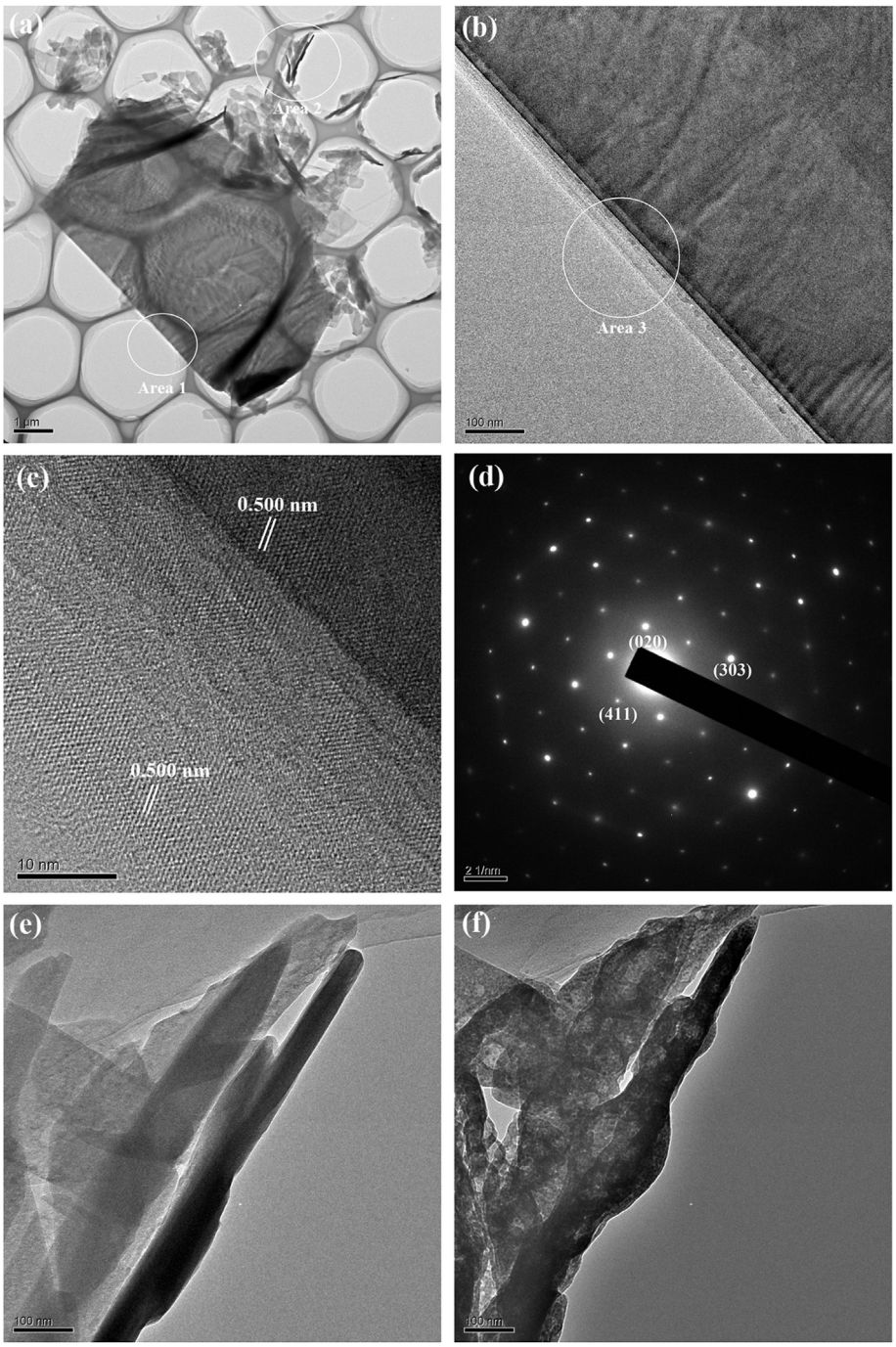

Fig. 3. TEM images of ZnO sample reacted with P_2 (a) for 24 h treatments (P/Zn molar ratio = 1.0); and HRTEM images (b, c and e) of selected areas pointed by Area 1, 3 and 2, respectively. Fig. 3d is the electron diffraction pattern of the area in Fig. 3c. Fig. 3f presents the Fig. 3e area after exposure to accelerating voltage (200 kV) for 5 s.

3.3. HRTEM analysis

Since XRD patterns suggested the presence of crystalline Zn-P precipitates, TEM analysis was conducted to obtain the detailed morphological and structural characterization of ZnO NPs as impacted by the four P species. We examined ZnO NPs before and after reaction with P species for 24 h (Figs. 3 and 4 and S2). Previous studies have reported the morphological changes of ZnO NPs in the presence of P_1 solution (Lv et al., 2012; Rathnayake et al., 2014). These reports found that the transformation products of ZnO NPs in P_1 solution were composed of orthorhombic hopeite, triclinic parahopeite, and the ZnO(crystalline)–$Zn_3(PO_4)_2$ (amorphous) core–shell structure, possibly as intermediates generated in the transformation process (Lv et al., 2012; Rathnayake et al., 2014).

TEM images of unreacted ZnO NPs showed rhombohedral morphology with 15–35 nm particle size (Figs. S2a and b). The presence of the crystalline ZnO NPs was evidenced by the presence of clear lattice fringes (~0.281 nm) corresponding to the (100) lattice planes and (100) faces were likely the dominant surfaces (Fig. S2b). Upon reaction with P_6, HTREM images still showed the presence of a crystalline material with lattice fringes (~0.281 nm) consistent with pristine ZnO NPs (Figs. S2c and d). This is in

agreement with XRD analysis which showed the dominant presence of ZnO NPs phase (Fig. 2d). However, the rhombohedral boundaries of the particles were altered and showed rounded features (Figs. S2c and d), suggesting that surface dissolution processes at least partially contributed to the chelation by P_6 (Fig. 1b and S2d).

TEM and HRTEM images of ZnO NPs reacted with P_2 revealed the presence of micrometer sized aggregations (Fig. 3a). This phase appeared to be crystalline with a measured lattice fringe distance of ~0.500 nm (Fig. 3c), consistent with the 5.00 Å d-spacing of the (311) planes of $Zn_2P_2O_7 \cdot 5H_2O$ as determined by XRD. Selected area electron diffraction (SAED) patterns (Fig. 3d) can be indexed with (020), (411) and (303) planes, further confirming that the final product is $Zn_2P_2O_7 \cdot 5H_2O$. Beam-induced morphological damage was observed when this phase was exposed to accelerating voltage (200 kV) for 5 s (Fig. 3e and f). This was possibly due to the co-existence of poorly crystalline Zn-P precipitates with structure similarity to $Zn_2P_2O_7 \cdot 5H_2O$ but with different hydration states, and/or the evaporation of water molecules from these phases upon interaction with high energy electron beam.

TEM micrographs of ZnO NPs particles reacted with P_3 showed the presence of two distinct types of particle morphology (Fig. 4a). First, the remaining ZnO NPs still had lattice fringes of ~0.281 nm as determined from the HRTEM images (Fig. 4b). The mean diameter (~30 nm) of the nanosized phase is similar with that of the unreacted ZnO NPs. Secondly, the newly formed aggregate phase is a crystalline material with lattice fringes of ~0.387 nm spacing (Fig. 4c and d), which is consistent with the 3.87 Å d-spacing of the (002) planes of $Zn_2HP_3O_{10}(H_2O)_6$ from XRD analysis (Fig. 2c).

3.4. Effect of pH and Zn/P ratio on P_3-induced transformation of ZnO NPs

ATR-FTIR spectra (1300–800 cm^{-1} region) and powder XRD patterns of ZnO-P_3 transformation products (i) at different reaction times (1–24 h) at pH 7.0, (ii) with different P_{-P3}/Zn molar ratios at pH 7.0, and (iii) at different pH levels (total P/Zn molar ratios = 1) are presented in Figs. 5 and 6. For ZnO-P_3 sample after 1 h reaction, three new bands appeared at 1137, 1140, and 928 cm^{-1} can be assigned to ν_{as}(P–O in Zn–PO_3^-), $\nu_{as}(PO_3)$, and ν_{as}(P–O–P), respectively (Fig. 5a). However, XRD analysis of the same sample did not show the presence of new peaks (Fig. 6a). These results suggested the possible formation of P_3 inner-sphere surface complexes with ZnO NPs at this reaction time (Yan et al., 2014). The FTIR spectra of ZnO-P_3 samples at 4, 10, and 24 h showed three new absorbance bands at 1240, 1106, and 991 cm^{-1} (Fig. 5a), which can be assigned to $\nu_{as}(PO_2)$ in bridging PO_2^-, ν_s(P–O) in terminal PO_3^{2-}, and $\nu_s(P_2O_7^{4-})$, respectively (Guan et al., 2005; Michelmore et al., 2003). Their XRD patterns showed the gradual presence of diffraction peaks consistent with $Zn_2HP_3O_{10}(H_2O)_6$ (Fig. 6a). FTIR spectra and XRD patterns of ZnO NPs reacted P_3 also showed similar results in the pH range of 5.0–9.0 (Fig. 6c). With decreasing solution pH or increasing reaction time, FTIR spectra and XRD patterns of the reaction products gradually showed the stretching vibration

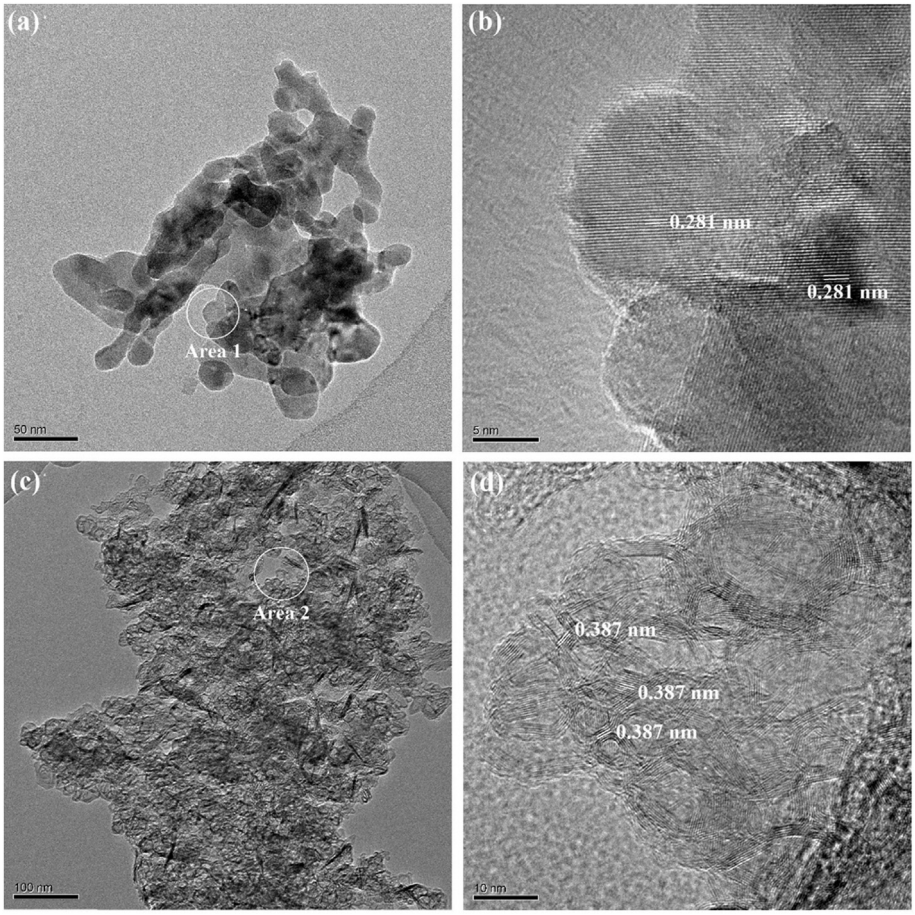

Fig. 4. TEM images of ZnO samples reacted with P_3 (a and c) for 24 h treatments (P/Zn molar ratio = 1.0); and HRTEM images (b and d) of selected areas pointed by Area 1 and 2, respectively.

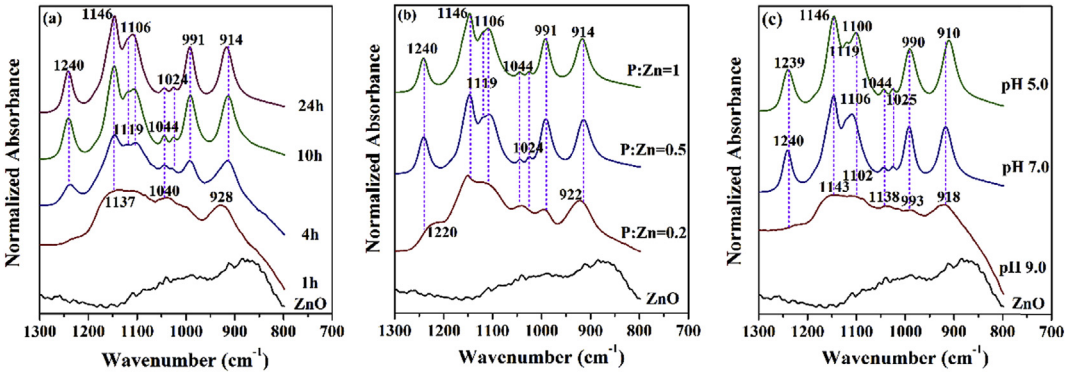

Fig. 5. Normalized ATR-FTIR spectra of P_3 reacted with ZnO NPs (a) with P_{-P3}/Zn molar ratios of 1:1 at pH 7.0 for different reactive time, (b) with three different P_{-P3}/Zn molar ratios at pH 7.0 at 24 h, and (c) with P_{-P3}/Zn molar ratios of 1:1 at different reactive pH at 24 h.

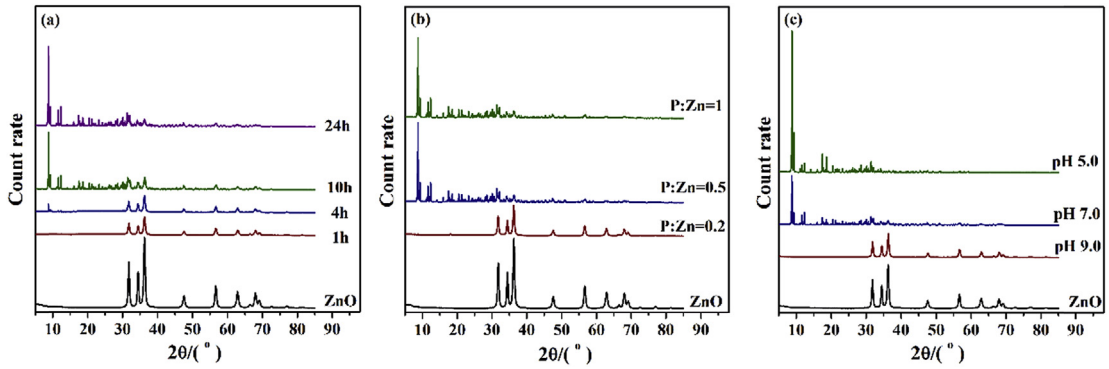

Fig. 6. XRD patterns of ZnO NPs reacted with P_3 (a) with P_{-P3}/Zn molar ratios of 1:1 at pH 7.0 for different reactive time, (b) with three different P_{-P3}/Zn molar ratios at pH 7.0 at 24 h, and (c) with P_{-P3}/Zn molar ratios of 1:1 at different reactive pH at 24 h.

and the diffraction peaks characteristic of $Zn_2HP_3O_{10}(H_2O)_6$ (Fig. 6a and b). Together, these observations suggested that $Zn_2HP_3O_{10}(H_2O)_6$ surface precipitates were formed on ZnO NPs following the formation of surface P_3 complexes and possibly the continuous dissolution of ZnO NPs. When the P/Zn molar ratio was 0.2, the FTIR spectra showed weak absorbance features of $Zn_2HP_3O_{10}(H_2O)_6$ precipitates with low intensity (Fig. 5b), while diffraction features of this phase were not detected in XRD (Fig. 6b). Possible explanations are the small amounts of this phase being under the detection limit of XRD (typically ~5%) and/or the formation of amorphous Zn-P_3 precipitates with structure similar to $Zn_2HP_3O_{10}(H_2O)_6$. These results suggested the formation of inner-sphere surface complexes and/or small coverage of possibly poorly crystalline surface precipitates at low P/Zn molar ratio (Yan et al., 2014). When the P/Zn molar ratio was higher than 0.2, both FTIR and XRD analysis of the reacted ZnO-P_3 samples clearly showed the presence of $Zn_2HP_3O_{10}(H_2O)_6$ precipitates. Taken together, these results revealed that the transformation of ZnO NPs was affected by reaction time, pH, and P/Zn molar ratio (Figs. 5 and 6).

4. Discussion and environmental implications

Previous studies have investigated the dissolution of ZnO NPs in the presence of different ligands, such as citric acid, phytic acid, fulvic acid, and humic acid (Bian et al., 2011; Feng et al., 2016; Jiang et al., 2015; Mudunkotuwa et al., 2012). Lv et al. (2012) and Rathnayake et al. (2014) investigated the effects of P_1 addition on the solubility and transformation of ZnO NPs (Lv et al., 2012; Rathnayake et al., 2014), and found the formation of amorphous $Zn(OH)_2$ coating on the surface of ZnO NPs. This amorphous $Zn(OH)_2$ phase was slightly soluble and resulted in the release of Zn^{2+} into solution. Aqueous PO_4^{3-} can be sorbed on the hydroxylated surface via exchange with OH^- or complexation with dissolved Zn^{2+} to form amorphous zinc phosphate hydrate precipitates, which eventually crystallized along with grain growth to form orthorhombic hopeite (Lv et al., 2012; Rathnayake et al., 2014). Polyphosphates are complex inorganic species with different numbers of phosphate groups, with the general formula being $(P_nO_{3n+1})^{(n+2)-}$ (Michelmore et al., 2003; Omelon and Grynpas, 2008). The objective of using different polyphosphates in the present study was to investigate the effects of different O–P–O linkages and chain lengths on the dissolution and transformation of ZnO NPs. The following reactions were likely involved: the initial hydroxylation and dissolution of the ZnO nanoparticle surface (eqs. (1) and (2)), the surface sorption of aqueous polyphosphates via ligand exchange (eq. (3)), the formation of soluble metal-phosphate complexes (eq. (4)), and the transformation of soluble Zn-P complexes into Zn-P precipitates (eq. (5)):

$$\equiv ZnO_{(s)} + H_2O_{(aq)} \Leftrightarrow \equiv Zn(OH)_{2(s)} \quad (1)$$

$$\equiv Zn(OH)_{2(s)} \Leftrightarrow Zn^{2+}{}_{(aq)} + 2OH^-{}_{(aq)} \quad (2)$$

$$\equiv Zn(OH)_{2(s)} + H(P_nO_{3n+1})^{(n+1)-}{}_{(aq)} \Leftrightarrow \equiv ZnH(P_nO_{3n+1})^{(n+1)-}{}_{(ads)} + 2OH^-{}_{(aq)} \quad (3)$$

$$Zn^{2+}{}_{(aq)} + H(P_nO_{3n+1})^{(n+1)-}{}_{(aq)} \Leftrightarrow ZnH(P_nO_{3n+1})^{(n-1)-}{}_{(aq)} \quad (4)$$

$$Zn^{2+}{}_{(aq)} + ZnH(P_nO_{3n+1})^{(n-1)-}{}_{(aq)} \Leftrightarrow Zn_2H(P_nO_{3n+1})^{(n-3)-}{}_{(s)} \quad (5)$$

In the presence of polyphosphates, the concentrations of dissolved Zn^{2+} changed with reaction time and was dependent on the structure and Zn-chelating capability of the different P species, which was consistent with previous research on bulk zincite (Michelmore et al., 2003). In that study, the concentration of Zn^{2+} in solution increased linearly with the addition of polyphosphate, but the concentration of dissolved Zn^{2+} was lower than our results at the same pH value (Michelmore et al., 2003). It is likely that the nano-sized ZnO particles in our study had higher solubility and released more Zn^{2+} for interaction with polyphosphates in solution (Mudunkotuwa et al., 2012). The previous study also mainly focused on the chemical adsorption of polyphosphates on the surface of zincite. The processes involving the Zn-polyphosphate surface complex transformation into Zn-polyphosphate precipitates were not revealed due to the low solubility of bulk zincite (Michelmore et al., 2003). Our study investigated both the sorption, precipitation, and/or transformation processes and products of polyphosphate interaction with ZnO NPs using a variety of microscopic and spectroscopic techniques.

Aqueous PO_4^{3-} can complex with dissolved Zn^{2+} ions and form amorphous zinc phosphate hydrate precipitate (Lv et al., 2012). The formation of these precipitates can decrease the concentration of free Zn^{2+} in solution, promote the continuous release of more Zn^{2+} from ZnO NPs, and finally transform into hopeite (Lv et al., 2012), which was pH dependent (Rathnayake et al., 2014). Because of the multiple phosphate groups within polyphosphates molecules, polyphosphates have great chelating ability especially for divalent metal cations (Omelon and Grynpas, 2008). Thus, polyphosphates can bind with a variety of metal ions to form soluble P complexes and finally transform into surface precipitates (Irani and Taulli, 1966; Yan et al., 2014). However, in this study, the rate and extent of Zn-phosphate precipitate formation did not increase with the increase number of phosphate groups in the four selected P compounds, but were rather controlled by the formation constants of metal-phosphate precipitates (Omelon and Grynpas, 2008; Wan et al., 2016). To our knowledge, the solubility product data for zinc-polyphosphates precipitates are not available in the literature. The free energy changes at 25 °C accompanying the association of Ca^{2+} with $P_2O_7^{4-}$, $HP_2O_7^{3-}$, and $HP_3O_{10}^{4-}$ were found to be −8.7, −4.9, and −5.3 kcal, respectively (Irani and Callis, 1960). Also, the dissociation constants of ferric pyrophosphate and ferric tripolyphosphate have been estimated to be $10^{-23.2}$ and $10^{-22.9}$, respectively (Irani and Morgenthaler, 1963). Therefore, P_2 might complex with Zn^{2+} more strongly than P_3 to form zinc-polyphosphates precipitates as suggested by our results. P_6 is typically considered to be an excellent complexing ligand, which can form stable and soluble complexes with metal ions (Andreola et al., 2004; Omelon and Grynpas, 2011). The concentration of dissolved Zn^{2+} in ZnO NPs-P_6 system was ~5 mmol L^{-1} (50% of total ZnO NPs) due to the presence of one terminal oxygen atom in each phosphate group of a P_6 molecule, likely resulting in a "caged" Zn-P_6 complex configuration with the Zn atom being octahedrally coordinated with the 6 terminal oxygen atoms.

The dissolution and transformation of ZnO NPs in the presence of polyphosphates and orthophosphate change the speciation of both Zn and P by forming Zn-P complexes and/or precipitates. The degree of effect (*e.g.*, enhancement *vs*. inhibition) of P compounds on the dissolution and transformation of ZnO NPs depends on the nature of the P species and solution conditions (*e.g.*, concentration and pH). Because TEM-revealed particle size of the reaction products was much larger than that of the initial ZnO NPs and the dissolved Zn^{2+} concentration was largely dependent on reaction time and P species, it is anticipated that the presence of phosphate and/or polyphosphates might change the toxicity of ZnO NPs in the environment (which is considered mainly due to dissolved Zn^{2+} and nanosize effects) (Li et al., 2011, 2013; Ma et al., 2013a).

In the samples from a pilot wastewater treatment plant (WWTP), $Zn_3(PO_4)_2$ ranged from 21% to 22% (Ma et al., 2014). However, the main components of Zn-P species in WWTP or natural systems are still unclear. Our study showed that the interaction mechanisms of ZnO NPs with various forms of P are very different and resulted in different reaction products. These results provide a new perspective for understanding the adsorption and precipitation behavior of polyphosphates and orthophosphate onto nano-sized ZnO materials (as compared to bulk materials) and the dissolution and microscopic transformation of ZnO NPs in P-enriched condition (Michelmore et al., 2003). It is thus important to include the transformation pathways and kinetics of nanoparticles under environmental conditions when considering their fate, transport, and toxicity. Taking into account the complexity of environmental components, future studies are still needed to (i) examine the effects of other environmentally relative components (*e.g.*, anions, organic acids, dissolved organic matter) on the transformation of ZnO NPs, (ii) identify the main component(s) and mechanism(s) of the Zn-P precipitates or soluble Zn-P complexes in environmental samples, and (iii) investigate the influence of such microscale morphological, structural, and compositional transformations on the bioavailability and toxicity (*e.g.*, plant uptake) of ZnO NPs and other similar metal oxide NPs under realistic environmental and exposure scenarios.

5. Conclusions

Our results suggested that P_2, P_3, and P_6 enhanced the dissolution of ZnO NPs, whereas P_1, P_2, and P_3 promoted the transformation of ZnO NPs into Zn-P precipitates through the interaction with dissolved Zn^{2+}. P_6 rapidly promoted the dissolution of ZnO NPs through the formation of soluble Zn-P complexes due to its excellent capability of chelating with metal ions instead of precipitating with them. Results from *in situ* ATR-FTIR, XRD, and HRTEM analyses indicated that at pH 7.0, the reaction products in the presence of P_1, P_2, P_3 are $Zn_3(PO_4)_2 \cdot 4H_2O$, $Zn_2P_2O_7 \cdot 5H_2O$, and $Zn_2HP_3O_{10}(H_2O)_6$, respectively. In addition, P_3 might form inner-sphere surface complexes on ZnO NPs at the beginning, and these surface complexes subsequently transform into Zn-P_3 precipitates. The dissolution and transformation of ZnO NPs obviously increased with increasing molar ratios of P_{-P3}/Zn and reaction time, and with decreasing solution pH.

Acknowledgements

We sincerely appreciate the constructive comments from the editor and anonymous reviewers, which greatly improved the quality of this manuscript. The authors gratefully acknowledge the National Natural Science Foundation of China (Grant Nos. 41471194 and 41171197), and the Strategic Priority Research Program of the Chinese Academy of Sciences (No. XDB15020402) for financial support of this research. Y. Tang acknowledges financial support

from Natural Science Foundation (Grant 1559087) and Georgia Water Resources Institute.

Appendix A. Supplementary data

Supplementary data related to this article can be found at http://dx.doi.org/10.1016/j.chemosphere.2017.02.134.

References

Andreola, F., Castellini, E., Manfredini, T., Romagnoli, M., 2004. The role of sodium hexametaphosphate in the dissolution process of kaolinite and kaolin. J. Eur. Ceram. Soc. 24, 2113–2124. http://dx.doi.org/10.1016/S0955-2219(03)00366-2.

Arai, Y., Sparks, D.L., 2007. Phosphate reaction dynamics in soils and soil components: a multiscale approach. Adv. Agron. 94, 135–179. http://dx.doi.org/10.1016/S0065-2113(06)94003-6.

Assaaoudi, H., Butler, I.S., Kozinski, J., Bélanger-Gariépy, F., 2005. Crystal structure, vibrational spectra and thermal decomposition of a new tetrazinc (II) dipyrophosphate decahydrate, $Zn_4(P_2O_7)_2{\cdot}10H_2O$. J. Chem. Crystallogr. 35, 49–59. http://dx.doi.org/10.1007/s10870-005-1154-7.

Barton, L.E., Auffan, M., Durenkamp, M., McGrath, S., Bottero, J.Y., Wiesner, M.R., 2015. Monte Carlo simulations of the transformation and removal of Ag, TiO_2, and ZnO nanoparticles in wastewater treatment and land application of biosolids. Sci. Total Environ. 511, 535–543. http://dx.doi.org/10.1016/j.scitotenv.2014.12.056.

Bian, S.W., Mudunkotuwa, I.A., Rupasinghe, T., Grassian, V.H., 2011. Aggregation and dissolution of 4 nm ZnO nanoparticles in aqueous environments: influence of pH, ionic strength, size, and adsorption of humic acid. Langmuir 27, 6059–6068. http://dx.doi.org/10.1021/la200570n.

Brunetti, G., Donner, E., Laera, G., Sekine, R., Scheckel, K.G., Khaksar, M., Vasilev, K., De Mastro, G., Lombi, E., 2015. Fate of zinc and silver engineered nanoparticles in sewerage networks. Water Res. 77, 72–84. http://dx.doi.org/10.1016/j.watres.2015.03.003.

Diaz, J., Ingall, E., Benitez-Nelson, C., Paterson, D., de Jonge, M.D., McNulty, I., Brandes, J.A., 2008. Marine polyphosphate: a key player in geologic phosphorus sequestration. Science 320, 652–655. http://dx.doi.org/10.1126/science.1151751.

Feng, X., Yan, Y., Wan, B., Li, W., Jaisi, D.P., Zheng, L., Zhang, J., Liu, F., 2016. Enhanced dissolution and transformation of ZnO nanoparticles: the role of inositol hexakisphosphate. Environ. Sci. Technol. 50, 5651–5660. http://dx.doi.org/10.1021/acs.est.6b00268.

Finstein, M.S., Hunter, J.V., 1967. Hydrolysis of condensed phosphates during aerobic biological sewage treatment. Water Res. 1, 247–254. http://dx.doi.org/10.1016/0043-1354 (67)90002-4.

Gong, W., 2001. A real time *in situ* ATR-FTIR spectroscopic study of linear phosphate adsorption on titania surfaces. Int. J. Min. Proces. 63, 147–165. http://dx.doi.org/10.1016/S0301-7516(01)00045-X.

Gottschalk, F., Sonderer, T., Scholz, R.W., Nowack, B., 2009. Modeled environmental concentrations of engineered nanomaterials (TiO_2, ZnO, Ag, CNT, fullerenes) for different regions. Environ. Sci. Technol. 43, 9216–9222. http://dx.doi.org/10.1021/es9015553.

Gottschalk, F., Sun, T., Nowack, B., 2013. Environmental concentrations of engineered nanomaterials: review of modeling and analytical studies. Environ. Pollut. 181, 287–300. http://dx.doi.org/10.1016/j.envpol.2013.06.003.

Guan, X.H., Liu, Q., Chen, G.H., Shang, C., 2005. Surface complexation of condensed phosphate to aluminum hydroxide: an ATR-FTIR spectroscopic investigation. J. Colloid Interface Sci. 289, 319–327. http://dx.doi.org/10.1016/j.jcis.2004.08.041.

He, Z., Honeycutt, C.W., Xing, B., McDowell, R.W., Pellechia, P.J., Zhang, T., 2007. Solid-State fourier transform infrared and ^{31}P nuclear magnetic resonance spectral features of phosphate compounds. Soil Sci. 172, 501–515. http://dx.doi.org/10.1097/SS.0b013e318053dba0.

Huang, R., Tang, Y., 2015. Speciation dynamics of phosphorus during (hydro)thermal treatments of sewage sludge. Environ. Sci. Technol. 49, 14466–14474. http://dx.doi.org/10.1021/acs.est.5b04140.

Huang, W., Cai, W., Huang, H., Lei, Z., Zhang, Z., Tay, J.H., Lee, D.-J., 2015. Identification of inorganic and organic species of phosphorus and its bio-availability in nitrifying aerobic granular sludge. Water Res. 68, 423–431. http://dx.doi.org/10.1016/j.watres.2014.09.054.

Irani, R.R., Callis, C.F., 1960. Metal complexing by phosphorus compounds. I. the thermodynamics of association of linear polyphosphates with calcium[1]. J. Phys. Chem. 64, 1398–1407. http://dx.doi.org/10.1021/j100839a010.

Irani, R.R., Morgenthaler, W.W., 1963. Iron sequestration by polyphosphates. J. Am. Oil Chem. Soc. 40, 283–285. http://dx.doi.org/10.1007/BF02633692.

Irani, R.R., Taulli, T.A., 1966. Metal complexing by phosphorus compounds—IX: thermodynamics of ionization of ortho-, pyro- and tripolyphosphoric acids. J. Inorg. Nucl. Chem. 28, 1011–1020. http://dx.doi.org/10.1016/0022-1902(66)80197-5.

Jiang, C., Aiken, G.R., Hsu-Kim, H., 2015. Effects of natural organic matter properties on the dissolution kinetics of zinc oxide nanoparticles. Environ. Sci. Technol. 49, 11476–11484. http://dx.doi.org/10.1021/acs.est.5b02406.

Keller, A.A., Lazareva, A., 2014. Predicted releases of engineered nanomaterials: from global to regional to local. Environ. Sci. Technol. Lett. 1, 65–70. http://dx.doi.org/10.1021/ez400106t.

Keller, A.A., Wang, H., Zhou, D., Lenihan, H.S., Cherr, G., Cardinale, B.J., Miller, R., Ji, Z., 2010. Stability and aggregation of metal oxide nanoparticles in natural aqueous matrices. Environ. Sci. Technol. 44, 1962–1967. http://dx.doi.org/10.1021/es90298 7d.

Klaine, S.J., Alvarez, P.J.J., Batley, G.E., Fernandes, T.F., Handy, R.D., Lyon, D.Y., Mahendra, S., McLaughlin, M.J., Lead, J.R., 2008. Nanomaterials in the environment: behavior, fate, bioavailability, and effects. Environ. Toxicol. Chem. 27, 1825–1851. http://dx.doi.org/10.1897/08-090.1.

Kołodziejczak-Radzimska, A., Jesionowski, T., 2014. Zinc oxide—from synthesis to application: a review. Materials 7, 2833–2881. http://dx.doi.org/10.3390/ma7042833.

Lampronti, G.I., Artioli, G., Oliva, L., Ongaro, A., Maretto, S., Bonino, F., Barbera, K., Bordiga, S., 2012. Role of phosphate species and speciation kinetics in detergency solutions. Ind. Eng. Chem. Res. 51, 4173–4180. http://dx.doi.org/10.1021/ie202 130y.

Li, M., Lin, D., Zhu, L., 2013. Effects of water chemistry on the dissolution of ZnO nanoparticles and their toxicity to *Escherichia coli*. Environ. Pollut. 173, 97–102. http://dx.doi.org/10.1016/j.envpol.2012.10.026.

Li, M., Zhu, L., Lin, D., 2011. Toxicity of ZnO nanoparticles to *Escherichia coli.*: mechanism and the influence of medium components. Environ. Sci. Technol. 45, 1977–1983. http://dx.doi.org/10.1021/es102624t.

Lowry, G.V., Gregory, K.B., Apte, S.C., Lead, J.R., 2012. Transformations of nanomaterials in the environment. Environ. Sci. Technol. 46, 6893–6899. http://dx.doi.org/10.1021/es300839e.

Lv, J., Zhang, S., Luo, L., Han, W., Zhang, J., Yang, K., Christie, P., 2012. Dissolution and microstructural transformation of ZnO nanoparticles under the influence of phosphate. Environ. Sci. Technol. 46, 7215–7221. http://dx.doi.org/10.1021/es301027a.

Ma, H., Williams, P.L., Diamond, S.A., 2013a. Ecotoxicity of manufactured ZnO nanoparticles – a review. Environ. Pollut. 172, 76–85. http://dx.doi.org/10.1016/j.envpol.20 12.08.011.

Ma, R., Levard, C., Judy, J.D., Unrine, J.M., Durenkamp, M., Martin, B., Jefferson, B., Lowry, G.V., 2014. Fate of zinc oxide and silver nanoparticles in a pilot wastewater treatment plant and in processed biosolids. Environ. Sci. Technol. 48, 104–112. http://dx.doi.org/10.1021/es403646x.

Ma, R., Levard, C., Michel, F.M., Brown Jr., G.E., Lowry, G.V., 2013b. Sulfidation mechanism for zinc oxide nanoparticles and the effect of sulfidation on their solubility. Environ. Sci. Technol. 47, 2527–2534. http://dx.doi.org/10.1021/es3035347.

Martin, M., Celi, L., Barberis, E., 1999. Determination of low concentrations of organic phosphorus in soil solution. Commun. Soil. Sci. Plant. Anal. 30, 1909–1917. http://dx.doi.org/10.1080/00103629909370341.

Michelmore, A., Jenkins, P., Ralston, J., 2003. The interaction of linear polyphosphates with zincite surfaces. Int. J. Min. Proces. 68, 1–16. http://dx.doi.org/10.1016/S0301-7516(01)00085-0.

Mudunkotuwa, I.A., Rupasinghe, T., Wu, C., Grassian, V.H., 2012. Dissolution of ZnO nanoparticles at circumneutral pH: a study of size effects in the presence and absence of citric acid. Langmuir 28, 396–403. http://dx.doi.org/10.1021/la203542x.

Murphy, J., Riley, J.P., 1962. A modified single solution method for the determination of phosphate in natural waters. Anal. Chim. Acta 27, 31–36. http://dx.doi.org/10.1016/S0003-2670(00)88444-5.

Omelon, S.J., Grynpas, M.D., 2011. Polyphosphates affect biological apatite nucleation. Cells Tissues Organs 194, 171–175. http://dx.doi.org/10.1159/000324845.

Omelon, S.J., Grynpas, M.D., 2008. Relationships between polyphosphate chemistry, biochemistry and apatite biomineralization. Chem. Rev. 108, 4694–4715 doi: 585 10.1021/cr0782527.

Pandurangan, M., Kim, D.H., 2015. In vitro toxicity of zinc oxide nanoparticles: a review. J. Nanopart. Res. 17 (158) http://dx.doi.org/10.1007/s11051-015-2958-9.

Rao, N.N., Gomez-Garcia, M.R., Kornberg 602, A., 2009. Inorganic polyphosphate: essential for growth and survival. Annu. Rev. Biochem. 78, 605–647. http://dx.doi.org/10.1146/annurev.biochem.77. 083007.093039.

Rathnayake, S., Unrine, J.M., Judy, J., Miller, A.F., Rao, W., Bertsch, P.M., 2014. Multitechnique investigation of the pH dependence of phosphate induced transformations of ZnO nanoparticles. Environ. Sci. Technol. 48, 4757–4764. http://dx.doi.org/10.1021/es404544w.

Reed, R.B., Ladner, D.A., Higgins, C.P., Westerhoff, P., Ranville, J.F., 2012. Solubility of nano-zinc oxide in environmentally and biologically important matrices. Environ. Toxicol. Chem. 31, 93–99. http://dx.doi.org/10.1002/etc.708.

Sivry, Y., Gelabert, A., Cordier, L., Ferrari, R., Lazar, H., Juillot, F., Menguy, N., Benedetti, M.F., 2014. Behavior and fate of industrial zinc oxide nanoparticles in a carbonate-rich river water. Chemosphere 95, 519–526. http://dx.doi.org/10.1016/j.chemosphere.2013.09.110.

Sun, T.Y., Gottschalk, F., Hungerbühler, K., Nowack, B., 2014. Comprehensive probabilistic modelling of environmental emissions of engineered nanomaterials. Environ. Pollut. 185, 69–76. http://dx.doi.org/10.1016/j.envpol.2013.10.004.

Uchimiya, M., Hiradate, S., 2014. Pyrolysis temperature-dependent changes in dissolved phosphorus speciation of plant and manure biochars. J. Agric. Food Chem. 62, 1802–1809. http://dx.doi.org/10.1021/jf4053385.

Wan, B., Yan, Y., Liu, F., Tan, W., Chen, X., Feng, X., 2016. Surface adsorption and precipitation of inositol hexakisphosphate on calcite: a comparison with orthophosphate. Chem. Geol. 421, 103–111. http://dx.doi.org/10.1016/j.chemgeo.2015.12. 004.

Wang, P., Menzies, N.W., Lombi, E., McKenna, B.A., Johannessen, B., Glover, C.J.,

Kappen, P., Kopittke, P.M., 2013. Fate of ZnO nanoparticles in soils and cowpea (*Vigna unguiculata*). Environ. Sci. Technol. 47, 13822–13830. http://dx.doi.org/10.1021/es40 3466p.

Worsfold, P.J., Monbet, P., Tappin, A.D., Fitzsimons, M.F., Stiles, D.A., McKelvie, I.D., 2008. Characterization and quantification of organic phosphorus and organic nitrogen components in aquatic systems: a review. Anal. Chim. Acta 624, 37–58. http://dx.doi.org/10.1016/j.aca.2008.06.016.

Yan, Y., Li, W., Yang, J., Zheng, A., Liu, F., Feng, X., Sparks, D.L., 2014. Mechanism of myo-inositol hexakisphosphate sorption on amorphous aluminum hydroxide: spectroscopic evidence for rapid surface precipitation. Environ. Sci. Technol. 48, 6735–6742. http://dx.doi.org/10.1021/es500996p.

Zhang, D.Q., Eng, C.Y., Stuckey, D.C., Zhou, Y., 2017. Effects of ZnO nanoparticle exposure on wastewater treatment and soluble microbial products (SMPs) in an anoxic-aerobic membrane bioreactor. Chemosphere 171, 446–459. http://dx.doi.org/10.1016/j.chemosphere.2016.12.05 3.

Zheng, X., Wu, R., Chen, Y., 2011. Effects of ZnO nanoparticles on wastewater biological nitrogen and phosphorus removal. Environ. Sci. Technol. 45, 2826–2832. http://dx.doi.org/10.1021/es2000744.